RSC Advances

RSC Publishing

PAPER

View Article Online
View Journal | View Issue

Cite this: *RSC Adv.*, 2013, **3**, 23673

Mesoporous TiO_2 as a nanostructured substrate for cell culture and cell patterning

Sangphil Park, Sung Hoon Ahn, Hyun Jong Lee, Ui Seok Chung, Jong Hak Kim and Won-Gun Koh*

Received 19th July 2013
Accepted 2nd October 2013

DOI: 10.1039/c3ra45136d

www.rsc.org/advances

We investigated the behaviors of mammalian cells such as adhesion, morphology and proliferation on mesoporous TiO_2-coated glass slides using NIH-3T3 fibroblasts as a model cell. A sol–gel process using amphiphilic poly(vinyl chloride) (PVC)-*g*-poly(oxyethylene methacrylate) (POEM) graft copolymer as a template produced defect or crack-free and homogeneous mesoporous TiO_2 films over a large area with high porosity and good connectivity. Cells grown on the mesoporous TiO_2 surfaces exhibited less spreading and had more filopodia than cells on the flat glass slides. The nanotopographical cues from the mesoporous TiO_2 resulted in the formation of more focal adhesions, promoting cell adhesion and proliferation without decreasing cell viability and functionality. We also demonstrated the capability of controlling spatial placement of cells onto chemically and topologically structured templates by fabricating poly(ethylene glycol) (PEG) hydrogel micropatterns on mesoporous TiO_2 films. Because a hydrogel precursor solution could infiltrate and become crosslinked within the multilayered mesoporous TiO_2 films, the resultant hydrogel micropatterns were firmly anchored on the substrate without the use of adhesion-promoting monolayers. While nanoscale topographic cues from mesoporous structure contributed to enhancement of cellular behaviors, different chemistry between cell-repelling PEG hydrogel and cell-adhesive mesoporous region facilitated confinement of cells on the micrometer scale. This study suggests that developed mesoporous TiO_2 films hold high potential for bioapplications showing high biocompatibility as surface coating materials for implants or as biomimetic platforms for cell patterning.

Introduction

Engineering cell–surface interactions using chemical and topographic cues is essential for the regulation of cellular characteristics such as cell adhesion, proliferation, morphology, and differentiation.[1–4] Specifically, nanoscale topographies have been considered to be promising biomimetic cell-stimulating cues because most cells *in vivo* are exposed to a nanostructured environment with complex topographical features composed of nanoscale pits, pores, protrusions, striations, particulates, and fibers.[5–9] As recent developments in advanced nanofabrication techniques have enabled the fabrication of substrates that are able to recapitulate the structure and length scale of the native topography, many studies have been carried out to investigate the role of surface topography in cell–material interaction, reporting that incorporation of nanotopography remarkably enhances cell and tissue functionality compared with a two-dimensional flat substrate.[10–14]

Among the various nanotopographical substrates, nanostructured titanium has recently emerged as a candidate biocompatible substrate due to its attractive features such as good stability in aqueous media and optical transparency.[15–19] For example, nanostructured titanium fabricated by surface mechanical attrition treatment (SMAT) enhanced the growth of mesenchymal stem cells (MSCs).[20] Schmuki *et al.* reported that viability, proliferation, and differentiation of MSCs are critically influenced by the nanoscale titanium oxide (TiO_2) surface topography with a specific response to nanotubes with diameters between 15 and 100 nm.[21] TiO_2 nanopowder-coated substrates were also used for *in vitro* characterization and investigation of osteoblasts responses.[22] Other attractive features of TiO_2 substrates include their photocatalytic properties, which enhance the hydrophilicity of substrates and facilitate self-cleaning such that the substrates are reusable after UV exposure.[23] In spite of those efforts to utilize nanostructured titanium substrate for cell-related studies, few studies have reported the use of multilayered and interconnected mesoporous TiO_2 films.[24]

In this study, we prepared mesoporous TiO_2 films using a graft copolymer consisting of a poly(vinyl chloride)(PVC) backbone and poly(oxyethylene methacrylate)(POEM) (PVC-*g*-POEM)

Department of Chemical and Biomolecular Engineering, Yonsei University, 50 Yonsei-ro, Seodaemun-gu, Seoul 120-749, South Korea. E-mail: wongun@yonsei.ac.kr; Fax: +82-2-312-6401; Tel: +82-2-2123-5755

as a structure-directing agent, and we utilized these materials as nanotopographic substrates for cell adhesion and growth. After the organized mesoporous TiO_2 films were coated onto the glass, their effects on cell behavior, such as cell adhesion, morphology, and proliferation, were investigated using fibroblasts as a model cell line. Furthermore, we demonstrated the capability of creating cellular micropatterns on mesoporous TiO_2 substrate by means of the spatial control of cell adhesion and proliferation using micropatterned PEG hydrogels.

Experimental section

Materials

Poly(ethylene glycol) diacrylate (PEG-DA) (MW 575), trypan blue solution (0.4%), 2-hydroxy-2-methylpropiophenone (HOMPP), titanium(IV) isopropoxide (TTIP), tetrahydrofuran (THF), Dulbecco's Modified Eagle's Medium (DMEM), fetal bovine serum (FBS), 3-(4,5-dimethylthiazol-2-yl)-2,5-diphenyltetrazolium bromide (MTT), antibiotic–antimycotic solution, trypsin/ethylenediaminetetra-acetate (trypsin/EDTA), Triton X-100, monoclonal anti-vinculin (mouse IgG1 isotype), and Tween-20 were purchased from Sigma-Aldrich (Milwaukee, WI, USA). A phosphate-buffered saline (PBS, pH 7.4) solution, Live/Dead Viability/Cytotoxicity Kit (L-7013), and ProLong Gold anti-fade reagent were purchased from Invitrogen (Carlsbad, CA, USA). FITC-conjugated secondary goat anti-mouse IgG antibody (FITC–Gt-Ms-IgG) and 4,6-diamidino-2-phenylindole (DAPI) were purchased from Merck Millipore (Bedford, MA, USA), and 4% paraformaldehyde in PBS (pH 7.4) and 10% goat serum were purchased from Wako (Osaka, Japan). Murine NIH-3T3 fibroblasts were obtained from the American Type Culture Collection (Manassas, VA, USA). Dulbecco's Phosphate-Buffered Saline (DPBS) was obtained from Thermo Scientific (Waltham, MA, USA). Amphiphilic poly(vinyl chloride) (PVC)-*g*-poly(oxyethylene methacrylate) (POEM) graft copolymer was synthesized as previously described.[25] The photomasks for photolithography were prepared using AUTO CAD and printed on transparencies using a standard laser jet printer.

Mesoporous TiO_2 substrate micropatterned with PEG hydrogel

Well-organized mesoporous TiO_2 films were prepared *via* a sol–gel process by using amphiphilic PVC-*g*-POEM graft copolymer as a template according to our previous report.[26,27] Briefly, PVC-*g*-POEM graft copolymer (PVC : POEM = 4 : 6 weight ratio) dissolved in THF (0.05 g per 1.5 mL) was added to 0.6 mL of precursor solution consisting of TTIP, H_2O, and HCl with molar ratio of 2 : 1 : 1. The resulting solution was aged at ambient temperature with stirring overnight and spin-coated onto a glass slide (1500 rpm, 30 s). Finally, calcination at 450 °C for 4 hours completely removed all organic chemicals, including the graft copolymer, to produce the organized mesoporous TiO_2 films. To create hydrogel micropatterns on the mesoporous TiO_2 films, a precursor solution consisting of 1 mL of 50% v/v PEG-DA and 20 μL of HOMPP was dropped onto the mesoporous TiO_2 substrates and then exposed to 365 nm, 300 mW cm^{-2} UV light source (EFOS Ultracure 100ss Plus, UV spot lamp, Mississauga, Ontario, Canada) through a photomask for 0.5 seconds.

Cell culture

The fibroblasts were cultured in 75 cm^2 polystyrene (PS) tissue culture flasks using DMEM with 10% FBS, and 1% antibiotic–antimycotic solution at 37 °C in a humidified atmosphere with 5% CO_2. To seed cells onto different substrates, cells were trypsinized from routine culture and centrifuged at 1000 rpm at 25 °C for 5 minutes. The concentrated cells were resuspended in fresh culture medium. An aliquot was obtained for cell counting in a hemocytometer to adjust the seeding density. Finally, approximately 1.0×10^5 cells were seeded onto each substrate and cultured under the same conditions.

Cell adhesion, proliferation, and viability

Cell adhesion was investigated by quantifying the cell area and the number of adhered cells. The cell areas were quantified using the ImageJ software package (NIH) to trace the cell cytoplasmic borders. To obtain the number of adhered cells on the substrates, the cells were detached by trypsin treatment. The detached cells were stained with trypan blue and counted by hemocytometer. Cell proliferation and viability were investigated with a Live/Dead Viability/Cytotoxicity fluorescence assay and an MTT assay as described previously.[28] The experimental conditions were same for both bare glass slide and mesoporous TiO_2. The area of both substrates was fixed at 1 cm × 1 cm and 1.0×10^5 cells per mL cells were seeded on both substrate. Five samples ($n = 5$) are represented for each data.

Scanning electron microscopy (SEM)

SEM images were obtained with a JEOL JSM-5600LV at 10 kV (JEOL, Ltd., Japan). All samples were sputter-coated with gold films with a thickness of 10 nm before observation. For cell morphology observation, the cells were washed with DPBS solution and fixed with 4% paraformaldehyde in PBS at 4 °C for 4 hours followed by dehydration through a series of gradient ethanol solutions (50, 70, 90, 95, and 100%) for 5 minutes each.

Atomic force microscopy (AFM)

AFM measurements on 100 nm × 100 nm area of mesoporous TiO_2 were made on a Dimension 3100/Nanoscope IVa (Digital Instruments, Santa Barbara, CA, USA) in tapping mode. Average roughness (RMS roughness) values were calculated from AFM using Gwyddion SPM data analysis software.

Immunostaining

DPBS containing 0.05% Tween-20 and DPBP containing 10% goat serum with 0.05% Tween-20 were prepared as a washing buffer and blocking agent, respectively. The cells were washed with DPBS to remove the cell-secreted factors and fixed with 4% paraformaldehyde in PBS (pH 7.4) for 10 minutes at room temperature. The fixed cells were rinsed twice with a washing buffer and then treated with 1% Triton X-100 in DPBS for

10 minutes. After rinsing three times with washing buffer, the cells were immersed with blocking agent for 30 minutes to reduce the non-specific binding. To visualize the focal adhesions, the cells were treated with anti-vinculin primary antibodies diluted 1 : 200 in DPBS for 1 hour. Then, the cells were rinsed three times for 5 minutes each with washing buffer and incubated with secondary antibody (FITC–Gt-Ms-IgG) at a dilution of 1 : 200 in DPBS for 1 hour. The stained cells were rinsed three times for 5 minutes each with washing buffer. Nuclei counterstaining was performed by incubating the cells with DAPI diluted 1 : 1000 in DPBS for 2 minutes at room temperature, followed by washing the cells twice with washing buffer, and the samples were subsequently immersed in DPBS for 5 minutes. All the specimens were mounted with ProLong Gold anti-fade reagent and covered with glass coverslips.

Fluorescence image acquisition and analysis

An inverted fluorescence microscope (Eclipse Ti) equipped with a Nikon Digital Sight (DS-Ri1) CCD camera (Nikon Inc. Garden City, NY) was used to obtain fluorescence images. The obtained images were imported as tiff files using the NIS-Elements F 4.00 software program (Nikon Inc.). The fluorescence images were then loaded into ImageJ and analyzed to calculate the cell areas and focal adhesion numbers per cell. The spread area of each cell was determined by using the freehand selections tool of ImageJ. After the areas containing the cell images were selected and masks for each cell were created, the mean areas of the cells on each sample were calculated. To quantify the number of focal adhesions and observe focal adhesion formation for each cell, immunofluorescence image planes of the cell bottom (cell–substrate interface) that clearly showed focal adhesions were selected for analysis. The vinculin image obtained from immunostaining was thresholded to produce a black and white focal adhesion image, from which the white pixels, representing focal adhesions, were counted and summed. The number of focal adhesions per cell was counted using the analyze particles function. All the results were quantitated by counting a minimum of 100 cells per sample.

Evaluation of protein adsorption

TiO_2 and PEG hydrogel-coated glass slides were immersed in serum-containing cell culture media at 37 °C for 24 hours. After washing and drying, the presence of adsorbed proteins from the cell culture media was investigated using X-ray photoelectron spectroscopy (XPS) (Kratos Analytical Inc., Chestnut Ridge, NY, USA).

Statistics

The data were compared using an independent two-sample *t*-test and *p*-values less than 0.05 were considered statistically significant.

Results and discussion

Mesoporous TiO_2 film coated on the glass substrate

The PVC-*g*-POEM graft copolymer was designed so that the hydrophilic POEM side chains can interact with the inorganic TiO_2 precursors, while a hydrophobic PVC backbone can produce a mesopore upon calcination. Synthesis of PVC-*g*-POEM graft copolymers and formation of PVC-*g*-POEM graft copolymer with microphase-separated micellar morphology was confirmed and discussed in our previous studies.[25,26] The resultant well-organized PVC-*g*-POEM graft copolymer was used as a template to synthesize mesoporous TiO_2 films *via* a sol–gel process based on the hydrolysis and condensation of TTIP. Because the precursor (TTIP) and its hydrolysis products preferentially incorporate into the POEM domains due to the favorable interactions between the TTIP and POEM chains, TiO_2 could be confined only in the POEM domains specifically and selectively, producing well-organized mesoporous TiO_2 films. SEM images confirm the formation of organized, multilayered mesoporous TiO_2 films with high porosity and good connectivity (Fig. 1a). The average pore size of the mesoporous TiO_2 films could be tuned from 30 nm to 70 nm by varying the weight ratio of PVC and POEM. In this study, the average pore size was fixed to approximately 30–50 nm because it was reported that cell proliferation, spreading, adhesion and viability might be impaired on a nanoporous substrate with a pore diameter larger than 50 nm. Resultant TiO_2 films had defect or crack-free mesoporous structures over large area as shown low magnification SEM image (Fig. 1b). Generally, organized mesoporous TiO_2 films have been synthesized *via* a sol–gel process using an amphiphilic block copolymer. However, the synthesis of block copolymers is very sensitive to impurities such as H_2O and O_2, requiring synthetic expertise and thus high cost. Use of a commercially available block copolymer, *e.g.*, Pluronic P123, often leads to TiO_2 with pore sizes smaller than 10 nm due to the low molecular weight of the copolymer, which impedes the complete crystallization while maintaining structural integrity. PVC-*g*-POEM graft copolymer is more advantageous than block

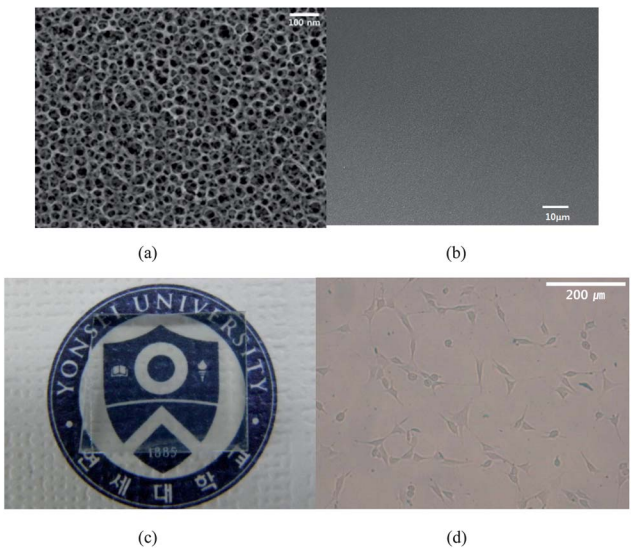

Fig. 1 Mesoporous TiO_2 films-coated on glass slides. (a) Top view SEM image of mesoporous TiO_2. (b) Low magnification SEM image of mesoporous TiO_2. (c) Photograph of TiO_2-coated glass slides maintaining optical transparency. (d) Optical image of fibroblasts cultured on TiO_2-coated glass slides.

copolymer due to the easy of synthesis and low cost. Also, the amorphous nature and high molecular weight (weight-average molecular weight, $M_w = 1.1 \times 10^5$ g mol^{-1}, polydispersity index, PDI = 2.2) of PVC-*g*-POEM can generate larger uniform mesopores, which promotes the complete titania crystallization while maintaining structural integrity. Thus, the amphiphilic PVC-*g*-POEM graft copolymer worked as a structure-directing agent not only on a mesoscopic scale, forming self-assembly of micelles, but also in macroscopic crystal growth of TiO_2, which allowed us to generate homogeneous mesoporous TiO_2 films over the large areas. The mesoporous TiO_2 films were highly transparent as shown in Fig. 1c, which allowed us to observe the cells with conventional optical microscopy (Fig. 1d). To investigate the variation of surface roughness between different samples, RMS roughness values of 10 different TiO_2 samples were measured using AFM. It was observed that the average and standard deviation of RMS roughness and standard deviation between the different samples were 36.4 nm and 5.3 nm, respectively.

Morphology of fibroblasts

To investigate the effect of surface topography on cell behaviors, we first observed the morphologies of fibroblasts. SEM was used to examine the morphology of the fibroblasts after 24 hours of culture on mesoporous TiO_2-coated and bare glass slides (Fig. 2a). Clear morphological differences were observed between the two substrates. The cells on the flat glass slides showed good spreading, changing from a polarized to flattened morphology, while cells on the mesoporous TiO_2 surfaces were less spread and were highly polarized with areas of dense filopodia extension. This result is consistent with other reports of cellular morphology on nanostructures.[11,29,30] The high magnification image shown in Fig. 2b confirmed that cells on the mesoporous TiO_2 had significantly more filopodia than cells on the flat glass slides. Quantification of the average cell area revealed that cells cultured on mesoporous TiO_2 had a significantly smaller area as shown in Fig. 2c. From these results, it appears that fibroblasts on the mesoporous TiO_2 produced a higher density of filopodia after adhesion and spent more time in interacting with substrates with the filopodia probing the nano-structured environment surrounding the cell, rather than spreading right after adhesion (as is apparent in cells on the flat glass slides).

Adhesion and proliferation of fibroblasts

Cell adhesion and proliferation were investigated by counting the number of cells per unit area on the mesoporous TiO_2-coated glass slides and the results were compared with cells seeded on bare glass slides. As shown in Fig. 3a, the fibroblasts grew well on both substrates, but cells on mesoporous TiO_2 substrates showed higher cell adhesion and proliferation rates when compared with cells on glass slides. The morphology study demonstrated that the area of cells on the glass slides was larger than on the mesoporous TiO_2 substrate. Therefore, on the glass slides, there was less available space for cell proliferation and more opportunities for the cells to contact each other,

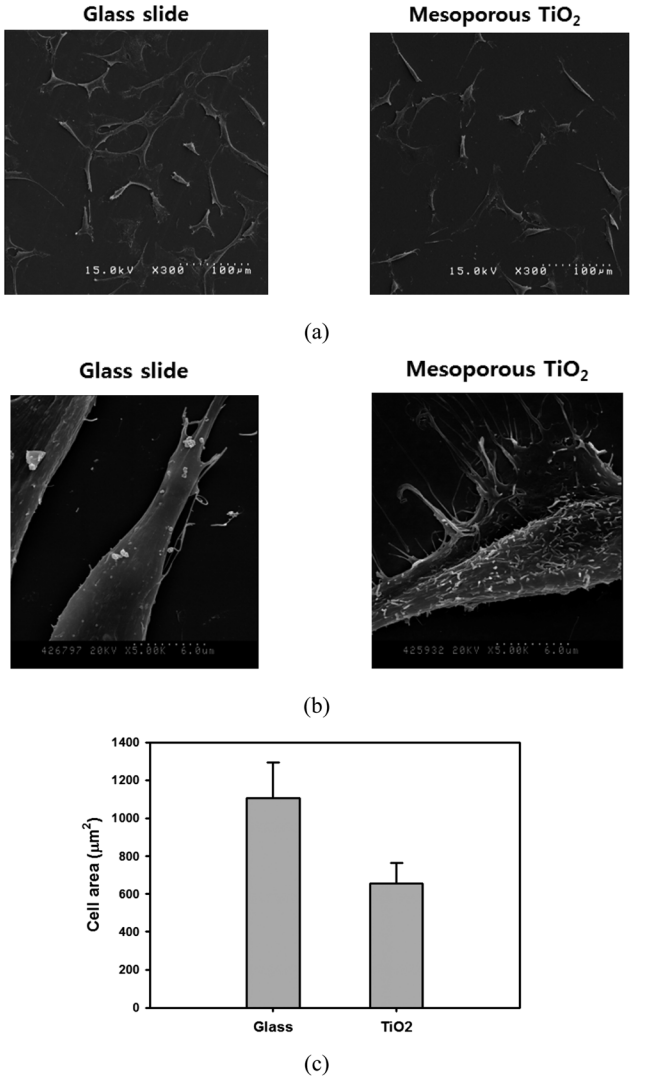

Fig. 2 Morphology of fibroblasts after 24 hours culture on bare glass slide and mesoporous TiO_2. (a) SEM images of fibroblasts. (b) High-magnified SEM image showing the different filopodia formation. (c) Quantitative analysis of cell area.

causing contact inhibition, which resulted in a decreased number of adhered cells and proliferation. In addition to cell adhesion, the cell viability during the period of cell–material interaction is extremely important because the cells may not be viable and functional in spite of higher adhesion and proliferation. We further investigated cell viability using the MTT assay. Fig. 3b shows that higher absorbance values were observed for mesoporous TiO_2 substrates than glass slides. However, when the absorbance was normalized with the number of adhered cells, similar values were obtained between two substrates. These results indicate that the nanoporosity or the well-defined nanoarchitecture on TiO_2 substrates seem to promote cell adhesion and proliferation, maintaining the same level of cell viability and functionality.

Analysis of focal adhesion

Focal adhesions are large and robust molecular complexes composed of several proteins involved in cellular signaling

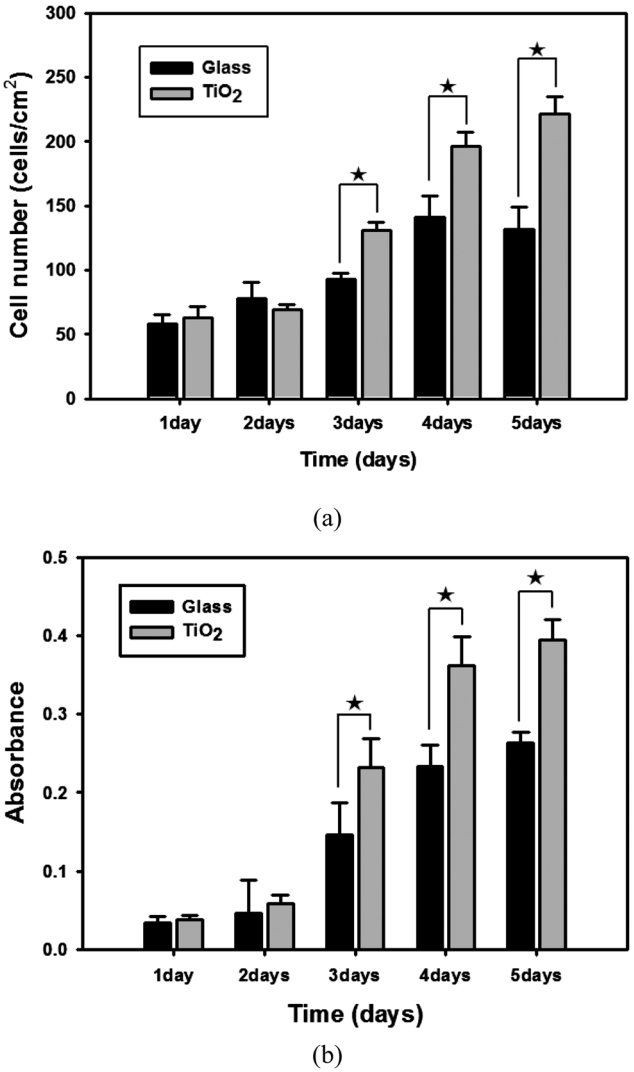

Fig. 3 Proliferation of fibroblasts adhered on bare glass slide and mesoporous TiO_2. (a) Change in the number of adhered cells as a function of culture time. (b) Result of MTT assay at different culture periods.

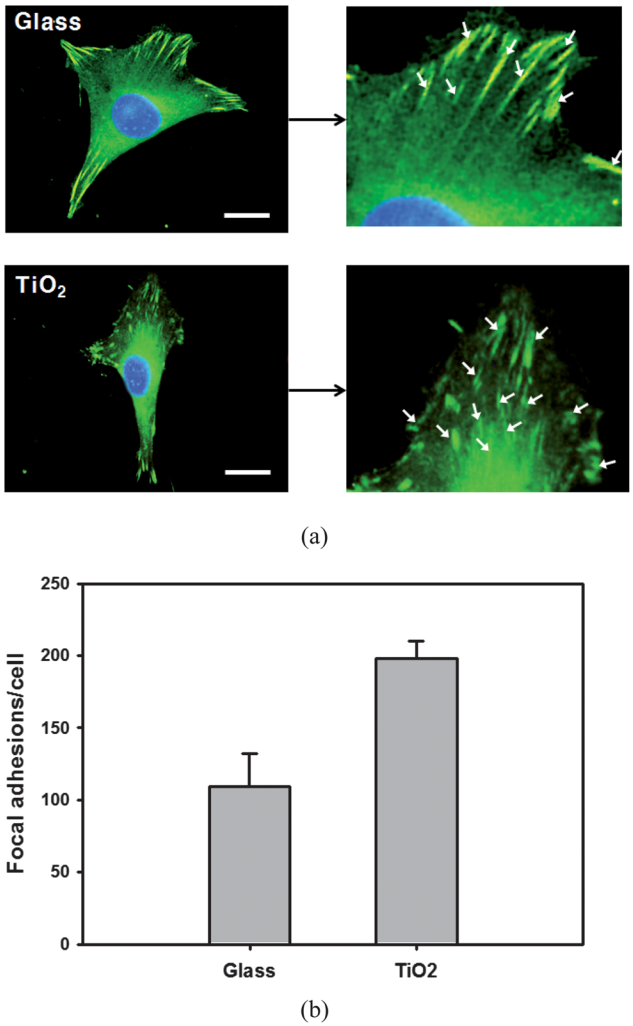

Fig. 4 Analysis of focal adhesions after 24 hours culture. (a) Immunostaining fluorescence images of focal adhesions (green: vinculin, blue: nucleus, scale bar: 20 μm). (b) Quantification of focal adhesions.

cascades, such as talin, vinculin, paxillin, and focal adhesion kinase.[31,32] The focal adhesion complex serves as a connector between actin filaments and integrins, which bind to the extracellular matrix (ECM).[14,33] Through focal adhesions, the cell senses a variety of environmental cues that affect many cellular characteristics, such as cell survival, ECM modification, intracellular tension, and cytoskeletal architecture.[34,35] To investigate the focal adhesions in detail, the cells on the glass slide and mesoporous TiO_2 substrates were incubated for 24 hours and immunostained for vinculin. Then, fluorescent images were obtained for the analysis of the spatial distribution and the number of focal adhesions. Fluorescence images revealed that most of the focal adhesion sites were dash-shaped and located at the cell periphery on the glass slides, whereas mesoporous TiO_2 substrates had more dot-shaped focal adhesion sites localized at central and peripheral regions of cells (Fig. 4a). When the number of focal adhesion sites was counted, we found that the cells on the mesoporous TiO_2 substrates had more focal adhesions per cell than cells on the glass slides (Fig. 4b). The number of focal adhesions is related to the affinity of cells for a substrate, as it was previously reported that stronger cell–substrate interactions lead to the development of more focal adhesion sites.[35] Therefore, these results imply that the cells might have a higher affinity for mesoporous TiO_2 substrates than for bare glass slides.

Cell patterning on the mesoporous TiO_2 substrate

After confirming that the adhesion and growth of fibroblasts were enhanced on the mesoporous TiO_2 substrate, hydrogel lithography was applied to develop arrays of microwells and subsequently to create cellular micropatterns. The array of microwells consisting of mesoporous TiO_2 at the bottom of each well and PEG hydrogel walls was fabricated by taking advantage of the abilities of PEG-DA to turn into a crosslinked hydrogel upon exposure to UV light and to create negative patterns *via* photolithography. Two different arrays of microwells with individual lateral dimensions of 200 × 200 μm and 50 × 50 μm,

arranged in 20 × 20 arrays, were fabricated. The SEM images demonstrate the formation of clearly defined hydrogel patterns without residual polymer inside the microwells, preserving the mesoporous structures of the TiO_2 substrates (Fig. 5a). Although micropatterned surfaces compartmented by PEG have been reported by many studies, most of them were prepared on flat substrates such as glass, silicon or gold *via* multi-step processes without providing nanotopographical cues to cells. Furthermore, when PEG hydrogel micropatterns were prepared on silicon or glass substrate, surfaces were modified by the self-assembly of alkoxy- and chlorosilanes with terminal acrylate and vinyl functional groups capable of taking part in the photoinitiated free-radical polymerization, resulting in covalent anchoring of hydrogel microstructures to the substrate.[28,36] Without such adhesion-promoting monolayers, hydrogel micropatterns are easily delaminated from the surface upon hydration due to swelling of the crosslinked hydrogel matrix. In this study, we prepared mesoporous TiO_2 substrates micropatterned with PEG hydrogel by single photopatterning process without any surface modification step. Using multilayered mesoporous TiO_2 film as a substrate for hydrogel micropatterns not only provide nanotopographical cues to cells but also eliminated the necessity for adhesion-promoting monolayer, because the hydrogel precursor solution was able to infiltrate and become crosslinked within the nanopores, thereby securely fixing the resultant hydrogel micropatterns to the substrate. It is well known that a PEG hydrogel can effectively prevent cell adhesion and spreading because it does not allow the protein adsorption that is a prerequisite for cell adhesion.[36] The protein adsorption on the surfaces of a PEG hydrogel and TiO_2 was investigated with XPS. Fig. 5b shows the XPS spectra for PEG hydrogel and TiO_2-coated glass slides that were incubated with serum-containing cell culture media. As shown in Fig. 5b, the XPS spectrum of a PEG hydrogel-coated substrate possessed a negligible N 1s peak, whereas strong N 1s signals were observed for the TiO_2-coated substrate due to the adsorption of more protein from the cell culture media. This difference in protein adsorption between the bottom of the microwell (mesoporous TiO_2) and the wall of the microwell (PEG hydrogel) was expected to allow spatial control of cells within the microwells. Fluorescence images of fibroblasts immobilized on micropatterned substrates were obtained from a fluorescent Live/Dead assay that stained the live cells green and dead cells red due to a difference in membrane permeability between live and dead cells. For both dimensions, cells adhered only to the interior of the microwells and the hydrogel walls served as effective barriers to cell adhesion and proliferation for 7 days (Fig. 6a). Although it was reported that cells within micropatterns could overgrow the cell resistant barrier and connected to cells within other micropatterns as culture time was prolonged,[37,38] microwells consisting of mesoporous TiO_2 bottoms and PEG hydrogel walls served as effective platform for cell patterning without any cross-over between micropatterned cells even for a long period of culture time. As was evident by the green emitted light, cells remained viable in different sizes of microwells. The fluorescence images also revealed that the cells formed a cellular cluster in both sizes of microwells after 5 days. The behavior of the cells on the micropatterned mesoporous TiO_2 substrate was further investigated using SEM and MTT analysis. According to the SEM images shown in Fig. 6b, the cells partially adhered and spread within the microwells in the early period of culture. After most of the area of the microwells was occupied by adhered cells, the cells tended to move away from the PEG hydrogel and a spheroid-like cell cluster was formed within both sizes of microwell. Due to the more limited cell adhesive area, fewer cells adhered and subsequently a smaller cellular cluster formed on a 50 μm microwell compared with a 200 μm microwell. The MTT assay demonstrated that the cells were able to proliferate within both sizes of microwells for up to 5 days, and their proliferation stopped after 5 days. Because of the larger available area for cell adhesion, the cells in the 200 μm microwells proliferated better than the cells in the 50 μm microwells. In the future, we will try to generate micropatterns of single cells by further reducing the size of microwell to understand single cell behaviors including proliferation on defined space of mesoporous TiO_2 layer surrounded by PEG without other cell interference/interaction.

The integration of a hydrogel micropattern into a mesoporous TiO_2 substrate allowed us to combine topological and chemical cues similar to those experienced by cells in their native environment, which elucidate the roles of topochemical

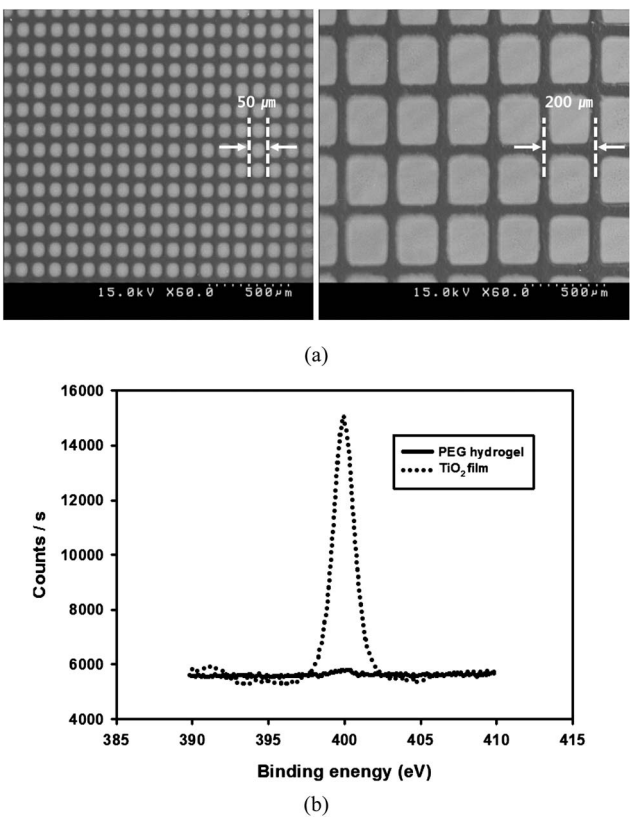

Fig. 5 Fabrication of array of microwells consisting of mesoporous TiO_2 and PEG hydrogel micropatterns. (a) SEM image of microwells with different lateral dimensions (50 × 50 μm, 200 × 200 μm). (b) N 1s peaks in XPS spectra obtained from PEG hydrogel and mesoporous TiO_2 surface that were incubated with serum-containing media.

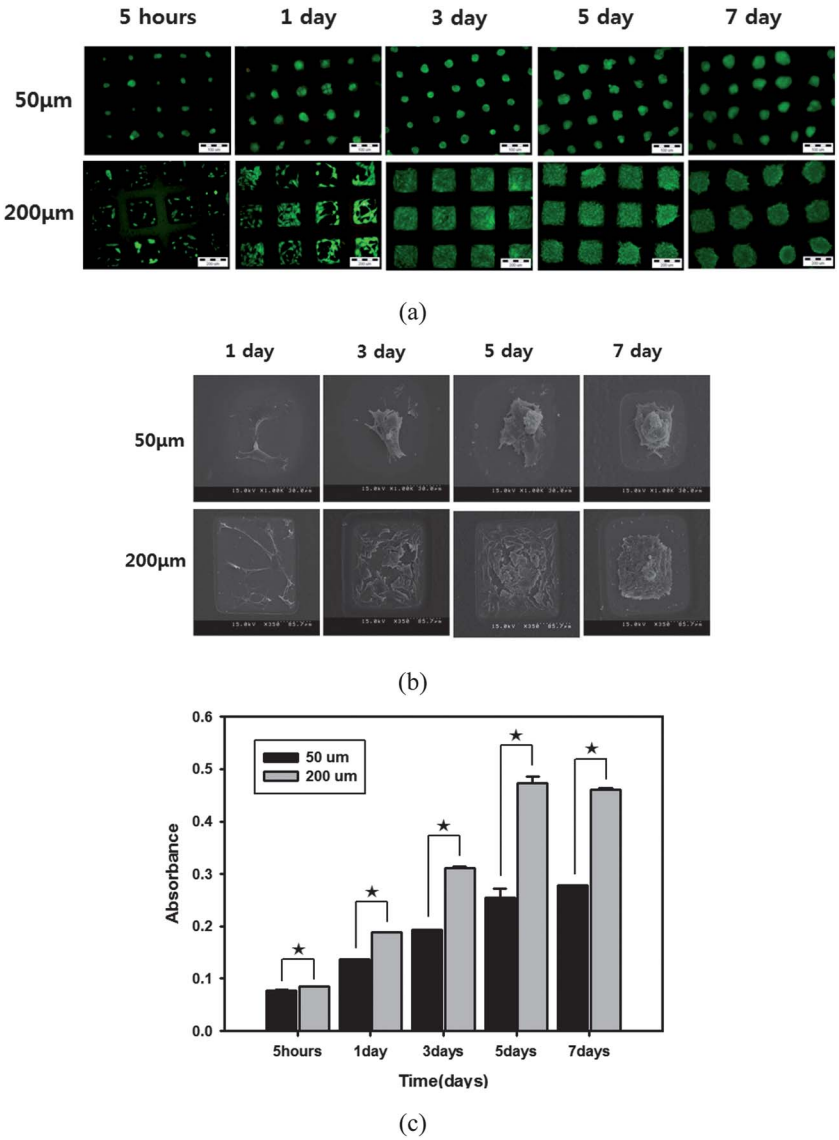

Fig. 6 Cellular micropatterns created on mesoporous TiO_2. (a) Live/dead fluorescence viability assay (scale bar: 100 μm for upper images and 200 μm for bottom images). (b) SEM images of fibroblasts cultured inside microwells having two different lateral dimensions (50 × 50 μm, 200 × 200 μm). (c) Result of MTT assay on micropatterned fibroblasts on two different sizes of microwells. (For cell patterning, 1.0×10^5 cells were seeded onto two different arrays of microwells with individual lateral dimensions of 200 × 200 μm and 50 × 50 μm, arranged in 20 × 20 arrays.)

cues in cellular functions. We demonstrated that topographic nanoscale cues contribute to the enhancement of cellular activity, and the differences in the chemical properties between the cell-repelling PEG hydrogel and the cell-adhesive mesoporous region facilitate confinement of the cells on the micrometer scale.

Conclusion

We investigated the effects of nanotopographic cue provided by mesoporous TiO_2 on the behaviors of fibroblasts such as morphology, adhesion and proliferation. *In vitro* tests confirmed that the mesoporous TiO_2-coated glass slide supported the formation of more filopodia, higher cell adhesion, proliferation, and viability when compared with normal glass slides. The fabrication of PEG hydrogel micropatterns on mesoporous TiO_2 substrates generated chemically structured template consisting of a cell-adhesive mesoporous TiO_2 region and a cell-repellent PEG hydrogel region. Because fibroblasts adhered and proliferated only on the mesoporous TiO_2, we could control the spatial placement of the cells onto chemically and topologically structured templates. It is clear from these model experiments that mesoporous TiO_2 has high potential for bioapplications such as surface coating materials for implants and substrates for cell microarrays with high biocompatibility and biomimetic environment.

Acknowledgements

This work was supported by the National Research Foundation (NRF) grant funded by the Ministry of Education, Science and Technology (MEST) (2011-0022709, 2010K001430 "Converging

Research Center Program", and 2007-0056566 "Active Polymer Center for Pattern Integration at Yonsei University").

References

1 N. J. Hallab, K. J. Bundy, K. O'Connor, R. L. Moses and J. J. Jacobs, *Tissue Eng.*, 2001, **7**, 55–71.
2 V. Hasirci and H. Kenar, *Nanomedicine*, 2006, **1**, 73–89.
3 M. Lampin, R. WarocquierClerout, C. Legris, M. Degrange and M. F. SigotLuizard, *J. Biomed. Mater. Res.*, 1997, **36**, 99–108.
4 M. Mrksich, *Chem. Soc. Rev.*, 2000, **29**, 267–273.
5 C. J. Bettinger, R. Langer and J. T. Borenstein, *Angew. Chem., Int. Ed.*, 2009, **48**, 5406–5415.
6 C. S. Chen, M. Mrksich, S. Huang, G. M. Whitesides and D. E. Ingber, *Science*, 1997, **276**, 1425–1428.
7 R. G. Flemming, C. J. Murphy, G. A. Abrams, S. L. Goodman and P. F. Nealey, *Biomaterials*, 1999, **20**, 573–588.
8 A. M. Lipski, C. Jaquiery, H. Choi, D. Eberli, M. Stevens, I. Martin, I. W. Chen and V. P. Shastri, *Adv. Mater.*, 2007, **19**, 553–557.
9 H. N. Kim, A. Jiao, N. S. Hwang, M. S. Kim, D.-H. Kang, D.-H. Kim and K.-Y. Suh, *Adv. Drug Delivery Rev.*, 2013, **65**, 536–558.
10 K. A. Simon, E. A. Burton, Y. B. Han, J. Li, A. Huang and Y. Y. Luk, *J. Am. Chem. Soc.*, 2007, **129**, 4892–4893.
11 M. J. Dalby, S. J. Yarwood, M. O. Riehle, H. J. H. Johnstone, S. Affrossman and A. S. G. Curtsi, *Exp. Cell Res.*, 2002, **276**, 1–9.
12 P. Decuzzi and M. Ferrari, *Biomaterials*, 2010, **31**, 173–179.
13 W. B. Tsai and J. H. Lin, *Acta Biomater.*, 2009, **5**, 1442–1454.
14 S. R. Ryoo, Y. K. Kim, M. H. Kim and D. H. Min, *ACS Nano*, 2010, **4**, 6587–6598.
15 J. Park, S. Bauer, A. Pittrof, M. S. Killian, P. Schmuki and K. von der Mark, *Small*, 2012, **8**, 98–107.
16 Y. Hu, K. Y. Cai, Z. Luo, D. W. Xu, D. C. Xie, Y. R. Huang, W. H. Yang and P. Liu, *Acta Biomater.*, 2012, **8**, 439–448.
17 A. S. Andersson, F. Backhed, A. von Euler, A. Richter-Dahlfors, D. Sutherland and B. Kasemo, *Biomaterials*, 2003, **24**, 3427–3436.
18 L. Z. Zhao, H. R. Wang, K. F. Huo, X. M. Zhang, W. Wang, Y. M. Zhang, Z. F. Wu and P. K. Chu, *Biomaterials*, 2013, **34**, 19–29.
19 S. Kaitainen, A. J. Mahonen, R. Lappalainen, H. Kroger, M. J. Lammi and C. J. Qu, *Biofabrication*, 2013, **5**, 025009.
20 M. Lai, K. Y. Cai, Y. Hu, X. F. Yang and Q. Liu, *Colloids Surf., A*, 2012, **97**, 211–220.
21 J. Park, S. Bauer, K. A. Schlegel, F. W. Neukam, K. von der Mark and P. Schmuki, *Small*, 2009, **5**, 666–671.
22 M. Hayashi, R. Jimbo, L. Lindh, J. Sotres, T. Sawase, K. Mustafa, M. Andersson and A. Wennerberg, *Acta Biomater.*, 2012, **8**, 2411–2416.
23 Y. Y. Song, F. Schmidt-Stein, S. Berger and P. Schmuki, *Small*, 2010, **6**, 1180–1184.
24 N. H. Harmankaya, J. Karlsson, A. Palmquist, M. Halvarsson, K. Igawa, M. Andersson and P. Tengvall, *Acta Biomater.*, 2013, **9**, 7064–7073.
25 S. H. Ahn, J. A. Seo, J. H. Kim, Y. Ko and S. U. Hong, *J. Membr. Sci.*, 2009, **345**, 128–133.
26 S. H. Ahn, J. H. Koh, J. A. Seo and J. H. Kim, *Chem. Commun.*, 2010, **46**, 1935–1937.
27 K. J. Son, S. H. Ahn, J. H. Kim and W. G. Koh, *ACS Appl. Mater. Interfaces*, 2011, **3**, 573–581.
28 W. G. Koh, A. Revzin and M. V. Pishko, *Langmuir*, 2002, **18**, 2459–2462.
29 M. J. Dalby, M. O. Riehle, D. S. Sutherland, H. Agheli and A. S. G. Curtis, *Biomaterials*, 2004, **25**, 5415–5422.
30 M. J. Dalby, S. Childs, M. O. Riehle, H. J. H. Johnstone, S. Affrossman and A. S. G. Curtis, *Biomaterials*, 2003, **24**, 927–935.
31 M. A. Schwartz and M. H. Ginsberg, *Nat. Cell Biol.*, 2002, **4**, E65–E68.
32 C. H. Seo, H. Jeong, K. S. Furukawa, Y. Suzuki and T. Ushida, *Biomaterials*, 2013, **34**, 1764–1771.
33 C. S. Chen, J. L. Alonso, E. Ostuni, G. M. Whitesides and D. E. Ingber, *Biochem. Biophys. Res. Commun.*, 2003, **307**, 355–361.
34 J. T. Parsons, A. R. Horwitz and M. A. Schwartz, *Nat. Rev. Mol. Cell Biol.*, 2010, **11**, 633–643.
35 M. Kato and M. Mrksich, *Biochemistry*, 2004, **43**, 2699–2707.
36 W. G. Koh, A. Revzin, A. Simonian, T. Reeves and M. Pishko, *Biomed. Microdevices*, 2003, **5**, 11–19.
37 C. S. Chen, M. Milan, S. Huang, G. M. Whitesides and D. E. Ingber, *Biotechnol. Prog.*, 1998, **14**, 356–363.
38 H. J. Lee, D. N. Kim, S. Park, Y. Lee and W. G. Koh, *Acta Biomater.*, 2011, **7**, 1281–1289.

